Large Eddy Simulation of Shallow Cumulus Convection during BOMEX: Sensitivity to Microphysics and Radiation

HONGLI JIANG AND WILLIAM R. COTTON

Department of Atmospheric Science, Colorado State University, Fort Collins, Colorado

(Manuscript received 9 February 1998, in final form 5 May 1999)

ABSTRACT

A number of large eddy simulations with the Regional Atmospheric Modeling System have been made to study the sensitivity of shallow marine cumulus convection to different microphysics and radiation schemes. In particular, the sensitivity of shallow marine cumulus convection to drizzle and radiation effects, and how drizzle and radiation modify turbulent fluxes, are investigated.

It is shown that for the case of prescribed radiative heating, drizzle—albeit very slight—leads to reduced buoyancy fluxes and less turbulence. Consequently, drizzling boundary layers appear to entrain less than their nondrizzling counterpart. Heavy drizzle events are simulated in association with deeper clouds as high as 2 km, even though the majority of clouds are only a few hundred meters deep. A heavier and longer lasting drizzle episode associated with a deeper boundary layer is produced when a two-stream radiative parameterization replaces the prescribed radiative heating in the simulation. Simulated surface precipitation rates agree reasonably well with observations. The greatest alteration in boundary layer structure is obtained when radiative heating interacts explicitly with the broadened drop distribution associated with drizzle formation.

1. Introduction

Accurate representation of cloud-related processes in general circulation and weather prediction models is a fundamental and challenging problem in atmospheric research, and the major objective of the Global Energy and Water Cycle Experiment (GEWEX) Cloud Systems Study (GCSS) program (Browning 1994).

As a participant of the GCSS intercomparison project Working Group 1, or boundary layer group, we have conducted large eddy simulations (LESs) of shallow cumulus convection that occurred during the Barbados Oceanographic and Meteorological Experiment (BOMEX) (Davidson 1968). Data collected during phase 3 (22–26 June 1969) of BOMEX are chosen for the shallow cumulus convection simulation. This period is marked by relatively undisturbed trade wind weather. It is a simple case that has no mesoscale complications and no transitions from cumulus to stratocumulus cloud. Nonetheless, radar observations provided a mean precipitation rate of 0.2 mm day^{-1} during the period of interest (Holland and Rasmusson 1973). As a rule of thumb, one would expect precipitation from trade wind cumuli in the region when they are greater than 2000 m deep (J. Simpson 1989, personal communication).

Data collected during BOMEX have been used in a number of studies. Siebesma and Cuijpers (1995) conducted LES of cases selected in BOMEX to evaluate assumptions widely made in parameterization of shallow cumulus convection. Soong and Ogura (1980) used a two-dimensional cloud model to investigate the response of shallow convective clouds to large-scale processes with BOMEX data for the undisturbed period.

Most studies of trade wind cumuli, both observational (e.g., Nitta and Esbensen 1974) and modeling (e.g., Nicholls and LeMone 1982; Siebesma and Cuijpers 1995), have focused their attention on the nonprecipitating nature of trade wind cumuli. Little research has addressed the role of precipitation and the changes of turbulent fluxes due to precipitation.

The primary focus of this research is to determine whether the simulated boundary layer cumulus clouds grow deep enough to allow drizzle to form. If so, will drizzle modify the distributions of turbulent fluxes? Furthermore, we are interested in whether including an interactive radiative parameterization in the simulation of shallow cumulus clouds will significantly alter the evolution and behavior of the cloud system and in how the radiation will interact with a drizzling boundary layer. In order to answer these questions, various sensitivity studies have been performed including microphysics and radiative effects.

Corresponding author address: Hongli Jiang, Department of Atmospheric Science, Colorado State University, Fort Collins, CO 80523-1371.
E-mail: jiang@pilsner.atmos.colostate.edu

The paper is organized as follows. Section 2 contains a summary of the LES model and experimental setup. Section 3 contains the description of the large-scale conditions and model initiation. Section 4 presents simulation results and sensitivity experiments to microphysics and the radiation scheme. Section 5 discusses the results and summarizes.

2. LES model and experimental setup

a. LES model

The LES model used in this study is a version of the Regional Atmospheric Modeling System (RAMS) developed at Colorado State University (Pielke et al. 1992). The highlights of model features are summarized in the following. The model is nonhydrostatic and compressible. The predicted variables include the three velocity components, the Exner function, the ice–liquid water potential temperature (Tripoli and Cotton 1981), and total water mixing ratio. An important feature of the bulk microphysical routines is that it has the capability of either predicting the mass mixing ratio of the hydrometeor species only (hereafter ''single-moment''; Walko et al. 1995) or predicting both mixing ratio and number concentration of species (''two-moment''; Meyers et al. 1997). In this purely warm cloud case, rain is the only predicted microphysical category while cloud water is diagnosed. The autoconversion scheme used is a newly developed scheme designed to provide a better estimate of autoconversion for low liquid water content boundary layer clouds (Feingold et al. 1998).

b. Radiation parameterization

A two-stream radiative transfer model is utilized for this study (Harrington et al. 1999). The two-stream model solves the equation of transfer for three gaseous constituents, H_2O, O_3, and CO_2, among which the CO_2 transfer includes climatological mixing ratio of CH_4, O_2, and NO_2. The gaseous absorption is calculated by following the fast exponential sum-fitting of transmissions method proposed by Ritter and Geleyn (1992). Lorenz–Mie theory is used to compute the optical properties for water drops, while the theory of Mitchell et al. (1996) is used for nonspherical ice crystals. For each hydrometeor species, the band-averaged values of optical properties are computed for the assumed gamma distribution function for each hydrometeor species used in RAMS following the method of Slingo and Schrecker (1982). Thus, for a given liquid water content, as condensed water is converted from cloud droplets to raindrops, the radiation model will calculate increased absorption.

c. Boundary conditions and numerical setup

Lateral boundaries are cyclic in both the east–west and north–south directions. The model top is a rigid lid. In order to minimize spurious reflection of upward propagating gravity waves, a Rayleigh friction absorbing layer is applied to the momentum equations and thermodynamic equation over the top five levels of the model (between 2800 and 3000 m) with damping timescale $\tau = 60$ s. The lower boundary is a material surface across which fluxes of heat, moisture, and momentum are prescribed; these fluxes will be given in the next section.

Simulations are done on a domain of $64 \times 64 \times 75$ grid points with a 100-m grid spacing in the horizontal and 40-m grid spacing in the vertical. The domain is thus 6400 m by 6400 m in the horizontal, and 3000 m in the vertical. A time step of 2 s is used in all integrations.

3. Case description and model initiation

The BOMEX event is chosen for this study in association with the intercomparison project of GCSS Working Group 1. The focus of this intercomparison study was nonprecipitating shallow marine trade wind cumulus convection. The model uses the standard configuration designed for the intercomparison to set up initial conditions and boundary conditions (hereafter this simulation is referred to as ''control run''). A detailed description of the case, the experiment design, and the large-scale forcing will be found online (www.knmi.nl/~siebesma/bomex.html) and in an upcoming paper (A. Siebesma et al. 1998, personal communication).

In the control run, the microphysics parameterization is switched off. The model allows condensation of water vapor to cloud water whenever supersaturation is attained. The partitioning of the total water substance into vapor and cloud water is diagnostic. No other forms of liquid or ice water are considered. Both the positive buoyancy effect of water vapor and the liquid water loading of cloud water are included in the vertical equation of motion.

The sensible and latent heat fluxes at the surface are prescribed as

$$\langle w'\theta' \rangle = \langle w'\theta_l' \rangle = 8 \times 10^{-3} \text{ K m s}^{-1} \quad (3.1)$$

$$\langle w'r_t' \rangle = \langle w'r_v' \rangle = 5.2 \times 10^{-5} \text{ m s}^{-1}, \quad (3.2)$$

where θ is the potential temperature, θ_l is the liquid potential temperature, and r_t and r_v are total water mixing ratio and water vapor mixing ratio, respectively. A prime denotes a departure from the domain average, and $\langle\ \rangle$ denotes the domain average.

The momentum fluxes are prescribed by

$$\langle u'w' \rangle = -u(u^{*2})/\sqrt{(u^2 + v^2)} \quad (3.3)$$

$$\langle v'w' \rangle = -v(u^{*2})/\sqrt{(u^2 + v^2)}, \quad (3.4)$$

where $u^* = 0.28$ m s^{-1}, and the velocities are the values at the lowest grid point level in the model.

In the control run, a large-scale subsidence with a

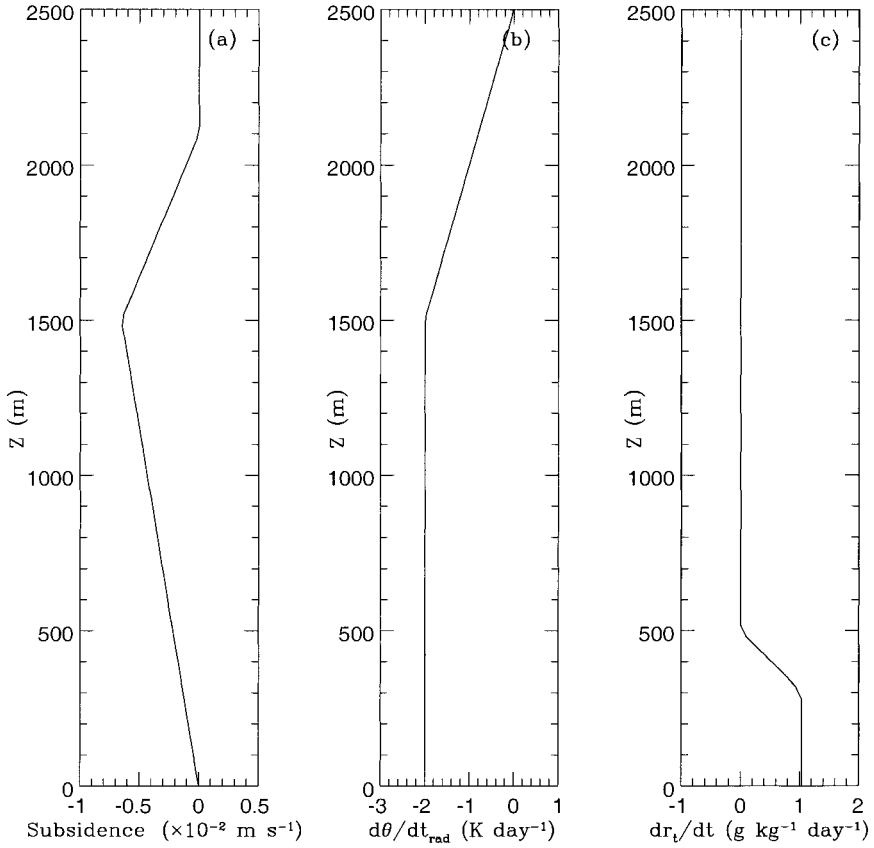

FIG. 1. Vertical profiles of the prescribed large-scale forcing: (a) large-scale vertical velocity (m s^{-1}), (b) radiative cooling (K day^{-1}), and (c) moisture tendency of total water (g kg^{-1} day^{-1}) in the subcloud layer.

maximum of -0.007 m s^{-1} is prescribed (Fig. 1a). A constant radiative cooling of 2 K day^{-1} (Fig. 1b) is imposed up to 1500 m, then decreases back to zero at 2500 m. The large-scale advective moisture tendency[1] of 1 g kg^{-1} day^{-1} is prescribed only in the mixed layer (Fig. 1c). The tendency of the subcloud layer water vapor mixing ratio due to the large-scale horizontal advective tendency is only about a 10th of the magnitude of the tendency due to the surface flux of water vapor. The initial potential temperature θ, horizontal wind u, geostrophic wind u_g, and total moisture r_t profiles are given in Fig. 2.

The initial θ and r_t profiles consist of three distinct layers: a well-mixed layer below 500 m, a conditionally unstable layer from 500 to 1500 m, and an absolutely stable inversion layer above 1500 m. The wind field is easterly throughout the domain with wind speeds equal to the geostrophic wind above the mixed layer. A westerly shear of 1.8×10^{-3} s^{-1} is in the initial wind. The initial v-component wind is set to zero.

4. Simulation results

Several experiments in addition to the control run have been performed in order to investigate the sensitivity of shallow marine cumulus convection to different microphysics and radiation parameterization. In order to understand how drizzle affects the turbulent fluxes and surface precipitation, we have repeated the control run with the inclusion of the single-moment microphysics (Walko et al. 1995) (hereafter ''drizzle run''). In the drizzle run, only the mixing ratio of rain is prognosed from the conservation equation that includes advective and turbulent transport by the resolved and subgrid velocities in the model, source (and sink) from hydrometeor type conversion, and sedimentation due to gravitation. The model initialization procedure, forcing, and configuration are identical to that in the control run.

It has long been known that radiative effects can significantly modulate the behavior of convective systems.

[1] Due to confusion with the experiment instructions, we inadvertently imposed the moistening tendency in the subcloud layer, whereas it should have been a drying tendency. B. Stevens (1998, personal communication) also inadvertently imposed the moistening tendency, then repeated the simulation with a drying tendency of equal magnitude, and found no significant change in the simulated clouds or fluxes.

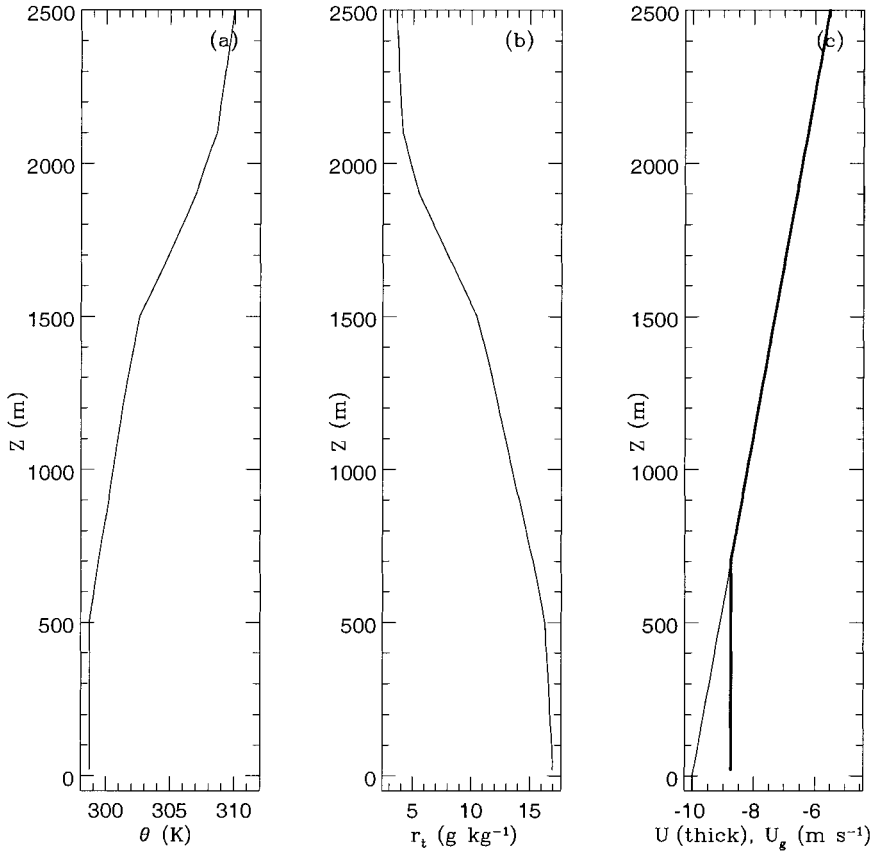

FIG. 2. Vertical profiles of the initial conditions: (a) dry potential temperature (K); (b) total water mixing ratio (g kg^{-1}); and (c) horizontal wind (heavy solid), geostrophic wind (thin solid) (m s^{-1}).

Most of the previous studies of radiative effects on cloud systems focus on deep convective systems (e.g., Dharssi et al. 1997; Tao et al. 1993). The radiative effect can be large for a stratocumulus-topped PBL as well because the cloud-top radiative cooling is often the major source for buoyancy production, and therefore for turbulent kinetic energy (TKE) (Moeng et al. 1996). We are interested in whether including an interactive radiative parameterization in the simulation of shallow cumulus clouds will significantly alter the evolution and behavior of the cloud system and in how the radiation will interact with a drizzling boundary layer. In order to answer these questions, we conduct two more simulations with a newly developed radiation parameterization (Harrington et al. 1999) replacing the prescribed radiative cooling (hereafter these two runs are referred to as ''control/rad'' and ''drizzle/rad,'' respectively). All other parameters remain the same as in the corresponding control or drizzle run. The experiments are summarized in Table 1.

The control run lasts 6 h. All of the additional runs start after the first hour of the control run and last for the remaining 5 h. An additional run with drizzle and a two-moment microphysics scheme was performed. Detailed comparison between ''drizzle/single-moment'' and ''drizzle/two-moment'' did not show significant differences, and thus no results from the drizzle/two-moment run will be shown. Comparison among all the runs in Table 1 will be presented.

It should be noted that two runs of the control case were performed with different initial random perturbations from the original control run to determine the statistical significance of the differences among the four cases. Detailed comparison of selected fields does not reveal significant differences; thus no results from these runs will be shown.

a. Time evolution

Selective model statistics are collected every minute; a subset of the statistics—containing cloud cover (the fraction of grid columns that contain cloud water), surface rain rate, cloud liquid water path (LWP), and vertically integrated TKE—is plotted as a time sequence in Fig. 3.

Both TKE $= \int_0^{z_T} \overline{\rho(z)}\,\overline{\mathrm{TKE}}\,dz$ and LWP $= \int_0^{z_T} \overline{\rho(z)}\,r_c\,dz$ are vertically integrated and horizontally averaged, where $\overline{\mathrm{TKE}} = 0.5 \times (\overline{u'^2} + \overline{v'^2} + \overline{w'^2})$, the horizontal

TABLE 1. Description of experiments.*

	Explicit microphysics	Radiation scheme
Control	No	Prescribe LW cooling
Drizzle	Single-moment	Prescribe LW cooling
Control/rad	No	Two-stream; Harrington et al. (1999)
Drizzle/rad	Single-moment	Two-stream; Harrington et al. (1999)

* See text for details.

bar denotes horizontal domain average, r_c is the cloud water mixing ratio, and z_T is the cloud-top height.

There is a two-hour initial spinup phase. During the spinup time period, no significant differences exist among all the runs. Model responses to various microphysical and radiative schemes are not yet established in the spinup period. All the fields show pronounced time variability, with two periods of generally enhanced values (after the spinup period), peaking near 180 and 280 min.

Cloud cover is about the same in all runs (Fig. 3a). After the spinup period, two heavy drizzle episodes with values of 1.4 and 1.2 mm day^{-1}, respectively, are simulated for the drizzle run (Fig. 3b). Both of them last approximately 20 min. Lighter drizzle persists in between the two heavy drizzle showers. Note that the surface rain rate and LWP show remarkably different evolution in the drizzle/rad run. One stronger drizzle event, lasting about 40 min, occurs at approximately 180 min from the beginning of simulation, with the maximum rate 2.4 mm day^{-1} (Fig. 3b). The surface rain rate is nearly zero for the rest of the simulation.

The maximum LWP (Fig. 3c) occurs at the same time as the heavy drizzle event and remains much lower afterward. The fact that cloud cover is about the same but the LWP has a drastic decrease in magnitude shows that regions having nonzero cloud water are about the same, but the cloud is much thinner because the heavy drizzle event has significantly reduced the liquid water content. The vertically integrated TKE (Fig. 3d) shows a similar trend as LWP: the maximum corresponds to the heavy drizzle event and remains steady thereafter in the drizzle/rad run.

The vertically integrated TKE in the control run exhibits a relatively quasi-steady nature for the last four hours of simulation except for a sudden increase to a maximum value that is almost twice as much as the average value near the end of the fifth hour (Fig. 3d). This appears to be due to more vigorous simulated cumulus cells at this time.

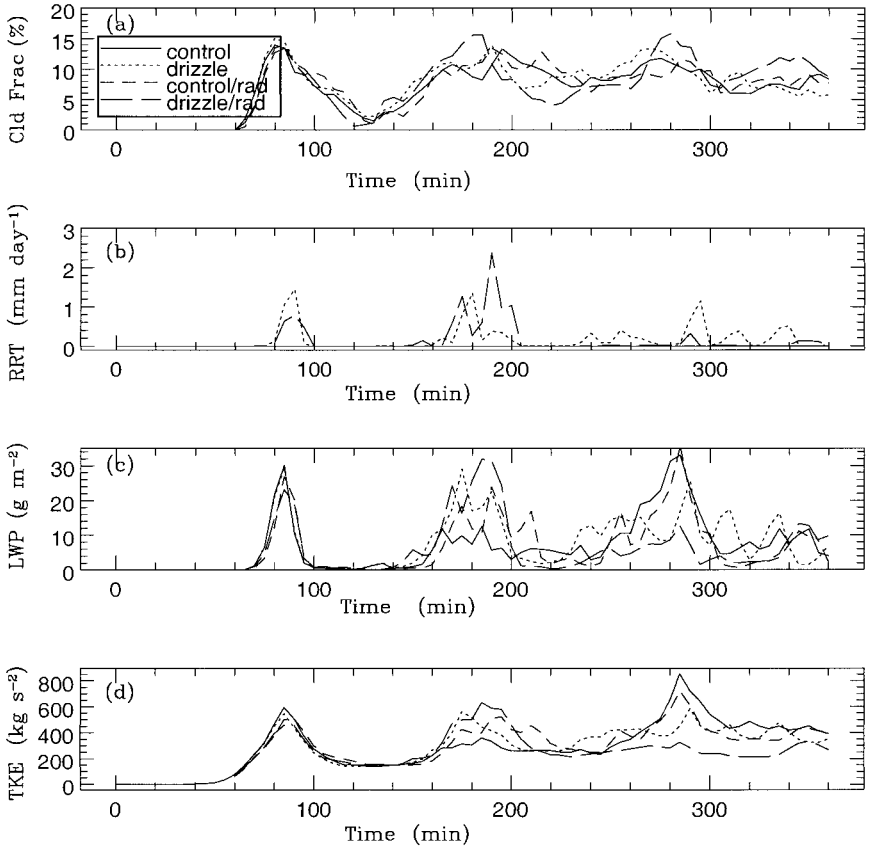

FIG. 3. Time evolution of domain-averaged (a) cloud fractional area, (b) surface rain rate (mm day^{-1}), (c) cloud liquid water path (LWP) (g m^{-2}), and (d) vertically integrated TKE (kg s^{-2}). See text for definitions.

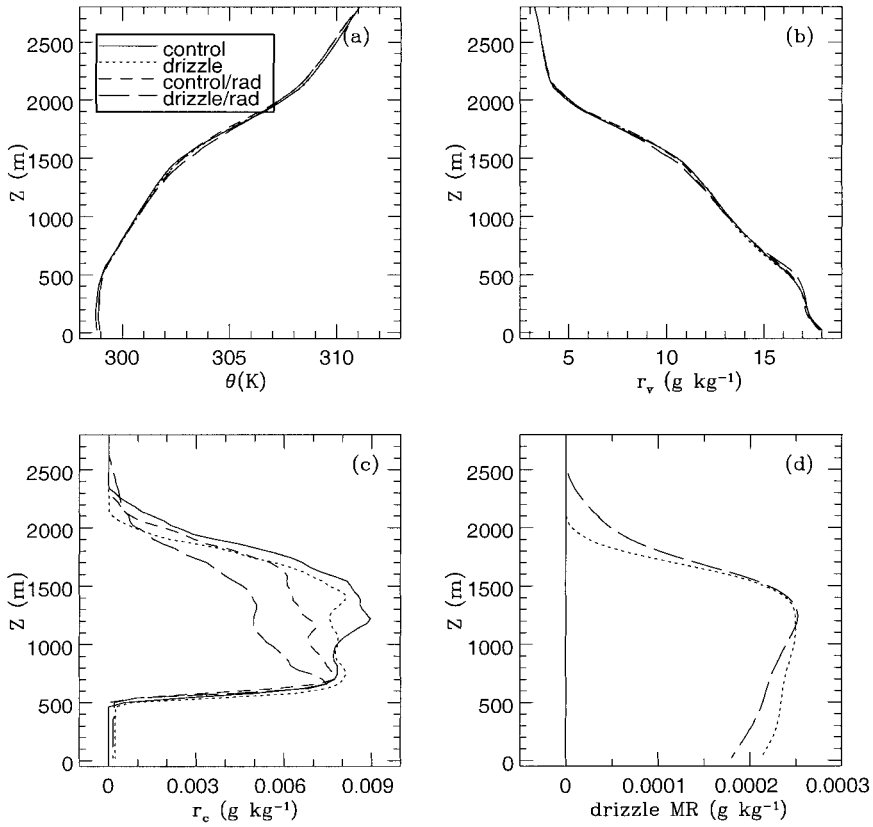

FIG. 4. Domain-averaged vertical profiles of (a) potential temperature, θ (K); (b) water vapor mixing ratio, r_v (g kg^{-1}); (c) liquid water mixing ratio, r_c (g kg^{-1}); and (d) drizzle mixing ratio (g kg^{-1}). All the fields in this and following figures, unless mentioned otherwise, are time-averaged over 3–6 h of simulation.

The averaged value of precipitation over the last four hours in both drizzle simulations is 0.18 mm day^{-1}, which agrees reasonably well with observations of 0.2 mm day^{-1} (Holland and Rasmusson 1973).

b. *Vertical profiles of mean cloud fields and turbulent fluxes*

The fields discussed in the following are averaged over the horizontal (x–y) planes and then time-averaged over the last three hours (3–6 h) of simulation.

The profiles of potential temperature θ and water vapor mixing ratio r_v (Figs. 4a,b) look almost identical among all the runs, with slight differences in the subcloud layer (below 500 m) and near the height of inversion (around 1500 m). The biggest differences (barely evident in Figs. 4a,b) are about 0.4 g kg^{-1} drying and 0.4 K warming near the inversion layer and about the same amount of moistening and cooling in the subcloud layer in the drizzle/rad run, compared to the control run. The net warming and drying that are present at the inversion layer suggest that the heavy drizzle event around the beginning of the fourth hour (see Figs. 3b,c) in the drizzle/rad run has effectively moved condensed water downward so that less evaporative cooling occurs at the inversion layer.

The drizzle mixing ratio has a maximum of 0.25×10^{-3} g kg^{-1} and decreases downward with height, reflecting the evaporation of falling drizzle in both the drizzle and drizzle/rad runs. Note that the height where drizzle mixing ratio becomes zero is about 500 m higher in the drizzle/rad run than that in the drizzle run. Furthermore, the decreasing drizzle mixing ratio with decreasing height below the maximum is more pronounced, suggesting stronger production of drizzle aloft and its stronger evaporation during fallout in the drizzle/rad run than in the drizzle run. The profiles of cloud water mixing ratio show that significantly different results are obtained when the prescribed longwave radiative cooling is replaced with the interactive radiation scheme. Drizzle production leads to an increased number of big drops and a decrease in liquid water content (LWC) in the vicinity of the cloud top as large drops sediment from that region. With radiative effects included, droplets grow rapidly due to radiative cooling at the cloud top, reducing water vapor amounts until subsaturation occurs. The differences between the control/rad and drizzle/rad result from the fact that droplets

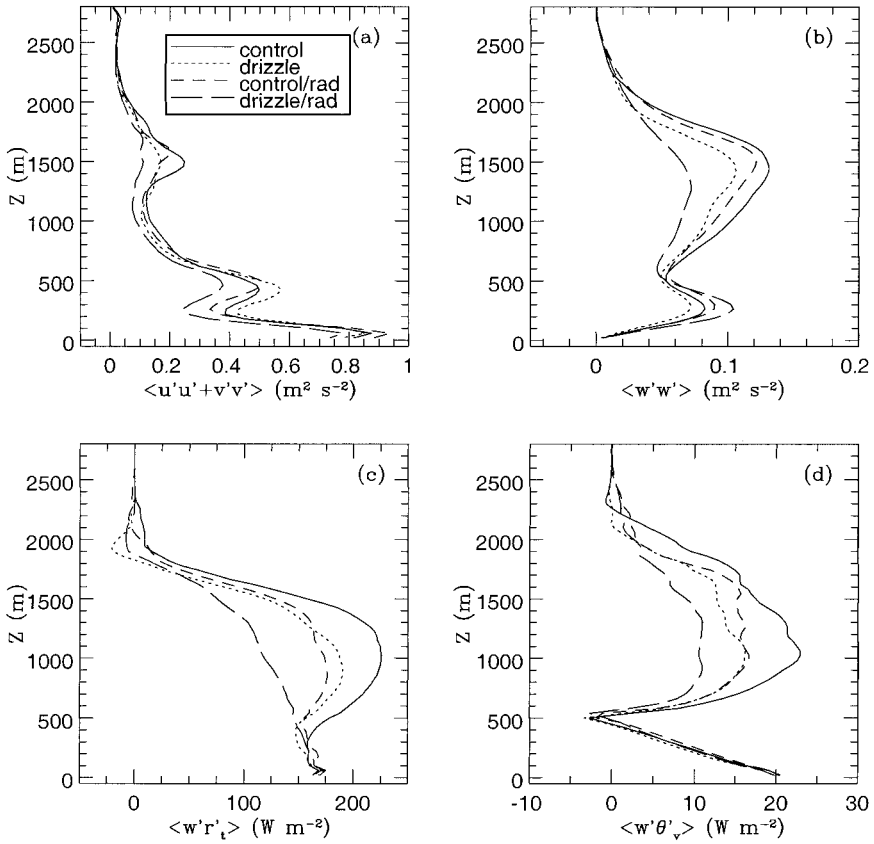

FIG. 5. Domain-averaged vertical profiles of (a) horizontal velocity variance ($m^2\ s^{-2}$), (b) vertical velocity variance ($m^2\ s^{-2}$), (c) total water fluxes ($W\ m^{-2}$) (resolved-scale plus subgrid-scale), and (d) total buoyancy fluxes ($W\ m^{-2}$) (resolved- plus subgrid-scale).

grow by condensation only and no sedimentation is activated in the control/rad run, while droplets grow bigger by both condensation and coalescence processes in the drizzle/rad run. The bigger droplets as well as the efficient removal of liquid water by the heavy drizzle result in the least amount of liquid water produced in the drizzle/rad run.

The horizontal velocity variance (Fig. 5a) is largest near the surface up to the lower part of the cloud layer (700 m) and comparable with that of the vertical velocity variance (Fig. 5b) aloft. The stronger drizzle aloft in the drizzle/rad run results in substantially reduced values of $\langle w'w' \rangle$ in the cloud layer, while the warm underlying surface contributes significantly to dry convective circulations in the subcloud layer resulting in a maximum in $\langle w'w' \rangle$ among all the runs.

The subgrid-scale flux of total water (not shown) has a maximum value of 150 $W\ m^{-2}$ near the surface and reduces to zero near 200 m. Above the surface, total water flux (including drizzle) has a nonlinear distribution in the control, control/rad, and drizzle runs, and a nearly linear distribution only in the drizzle/rad run. The nonlinear distributions of total water flux suggest that these simulations have not reached a statistically quasi–steady state. The total water flux is the strongest in the cloud layer in the control run while the surface value remains the same. The stronger flux in the control run is related to dry air being entrained downward causing a flux increase over time, which also suggests that more entrainment takes place with time. The cause of the small negative fluxes in the layer near 2000 m in the drizzle run is not clear.

Like the total water fluxes, the subgrid-scale buoyancy fluxes (not shown) dominate the total buoyancy fluxes near the surface. In all runs the total buoyancy fluxes (Fig. 5d) decrease with height in the subcloud layer from a surface value of 20 $W\ m^{-2}$ to near zero around 500 m, then reach a maximum around 1000 m in the cloud layer. The strongest cloud layer maximum is produced in the control run and the weakest is produced in the drizzle/rad run. The small negative value near 2000 m in the control run may be related to the warmer air above moving down due to entrainment. Near cloud base the air is statically stable (Stull 1988); therefore, a minimum value in buoyancy flux is simulated in all runs.

The analysis of the resolved TKE budgets (Fig. 6) reveals that the major source of TKE from the surface to 100 m is from shear production (Fig. 6a) among all the runs. The buoyancy production term (Fig. 6d) is the

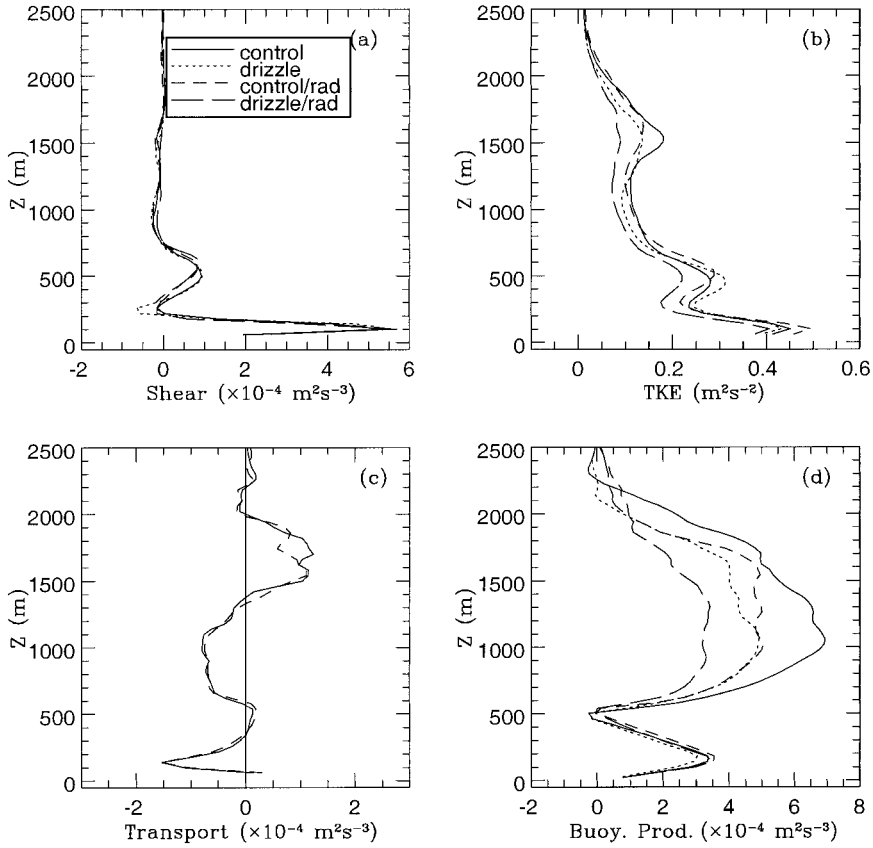

FIG. 6. Vertical profiles of various terms in TKE budgets: (a) shear production, (b) resolved-scale TKE ($m^2\ s^{-2}$), (c) transport, and (d) buoyancy production. All budget terms are in the unit of $m^{-2}\ s^{-3}$.

major source of TKE in the cloud layer. The control run has a much larger buoyancy production of TKE, part of which is being transported upward in layers between 1300 and 2000 m where a maximum TKE is produced, and part of which is transported downward in a deep layer from the surface to 1300 m, resulting in a minimum in the cloud layer and maximum in the subcloud layer. The stronger buoyancy forcing, and therefore stronger TKE, in the control run induces a larger entrainment rate (Moeng et al. 1996).

c. Vertical profiles of conditionally sampled cloud fields and fluxes

We have shown thus far that drizzle, especially the interaction between drizzle and radiation, has some impact on the domain-averaged cloud fields and turbulent fluxes. In order to better understand how drizzle and the interaction between drizzle and radiation affect the fluxes and cloud evolution, the cloud fields described below are conditionally sampled and averaged separately over the cloud updraft and downdraft regions. The cloud updraft (downdraft) region is defined as all grid points with cloud water and positive (negative) vertical velocity. This has proved to be a useful way to partition parameters in cases where the cloud mass fluxes of downdraft become comparable with the cloud updraft (Tiedtke 1989).

The vertical profiles of cloud fractional area (fraction of grid points that contain cloud water over the entire domain) and conditionally sampled cloud liquid water, drizzle mixing ratio, and vertical velocity in the cloud updraft region are shown in Fig. 7. The cloud fractional area (calculated with cloud water only; Fig. 7a) is similar among all the runs except that the drizzle/rad run has slightly less cloud coverage in the cloud layer and about 1% more near cloud base. When both drizzle and cloud water mixing ratio are included in the calculation (not shown), the greatest differences occur near the cloud base and in the subcloud layer due to the presence of falling drizzle. In general, the cloud cover decreases with height very quickly from its maximum near cloud base (around 500 m) to one-third of its maximum in the vicinity of 800 m, suggesting that most of clouds are shallow with cloud depth a few hundred meters, and only 1% reach as high as 1500 m in all the runs. The maximum cloud coverage is ~6%–7%. These results agree well with the study of Nicholls and LeMone (1980), who found with the data collected during GATE phase III that on undisturbed days, cloud base was about

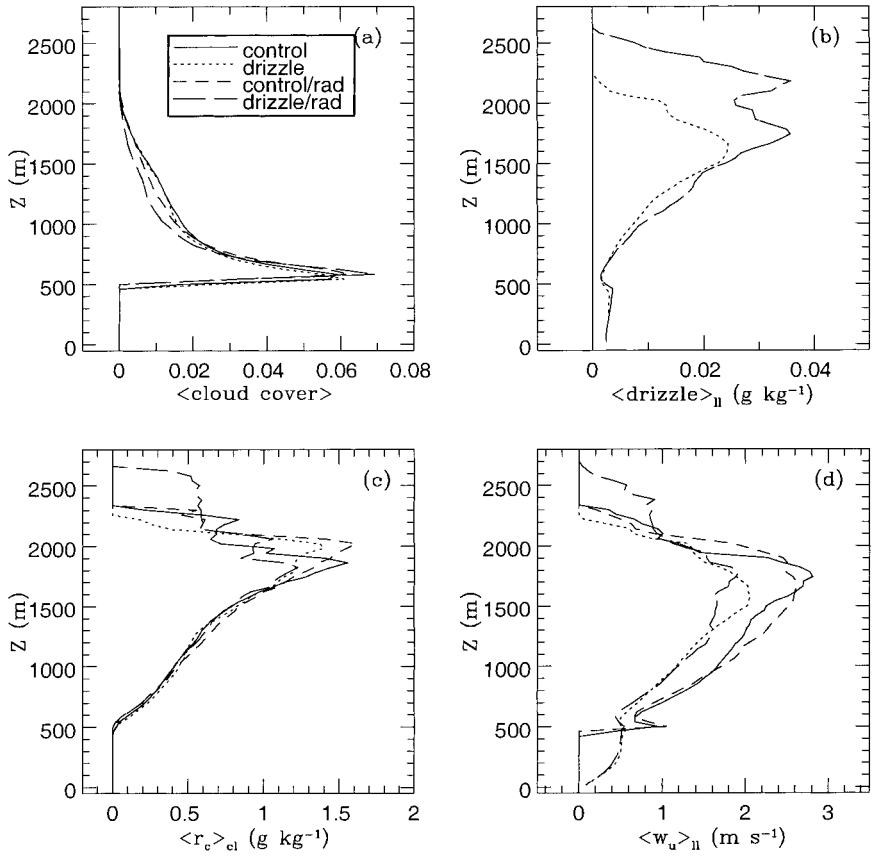

FIG. 7. (a) Vertical profile of cloud cover (fraction of grid points that contain cloud water over the entire horizontal domain). Vertical profiles of (b) drizzle mixing ratio (g kg^{-1}), (c) cloud water mixing ratio (g kg^{-1}), and (d) vertical velocity (m s^{-1}) conditionally sampled and averaged over the cloud updraft region. The subscript $\langle\ \rangle_{cl}$ in this and following figures denotes conditionally sampled in the cloud updraft region. The subscript $\langle\ \rangle_{ll}$ in this and following figures denotes conditionally sampled in the cloud updraft region with inclusion of rain water.

500 m, cloud height about 1000 m, and cloud cover about 10%.

The vertical distribution of drizzle mixing ratio in the cloud updraft region (Fig. 7b) shows clearly that the few clouds reaching the inversion layer are drizzle-producing clouds. The maximum drizzle mixing ratio is located near the inversion layer. There is a very small amount of drizzle in the downdraft region (not shown). Note that only a small amount exists in the subcloud layer as well. Of particular interest is that the drizzle mixing ratio in the drizzle/rad run is about 50% more in the upper levels and about 400 m deeper than in the drizzle run. It is known that the deeper the cloud, the more likely it is for the production of large droplets capable of initiating the collision–coalescence process, and therefore more droplets grow to a radius of drizzle size by condensation and coalescence (Mason 1971).

The most striking feature in the vertical profiles of cloud liquid water mixing ratio in the cloud updraft region (Fig. 7c) is the change in cloud-top characteristics in the drizzle/rad run with little differences in the cloud layer among all the runs. In particular, the level where the cloud top disappears is about 400 m higher in the drizzle/rad run, compared to other runs. When the time average is taken for each individual hour for the last three hours of simulation (not shown), the level where cloud top disappears in the drizzle/rad run lowers from 2700 to 1900 m (800-m net decrease), whereas the height only decreases about 200 m in the drizzle run. A much deeper cloud is simulated prior to the heavy drizzle event in the drizzle/rad run. The heavy drizzle event (Fig. 3b, long-dashed line) occurs simultaneously with the time when cloud is the deepest, exceeding 2000 m (consistent with Simpson's rule of thumb in the region). From aircraft observations made during suppressed conditions near Puerto Rico, Pennel and LeMone (1974) reported that the aircraft encountered rain at 980 m, while cloud tops were never observed to exceed 2000 m. Only minor differences are found between the control run and control/rad run. The height experiences a net increase in the control run (from 1900 to 2100 m), suggesting more entrainment takes place there, whereas the height experiences an increase–decrease cycle during the 3-h time period and the net

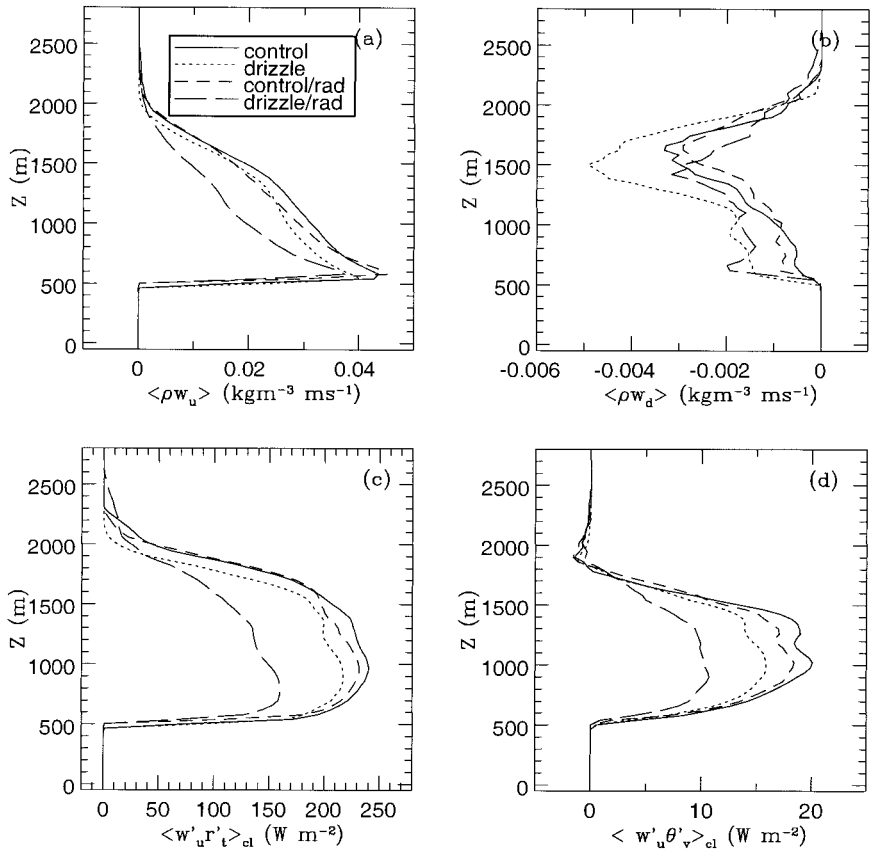

FIG. 8. Vertical profiles of (a) upward cloud mass flux (kg m^{-3} m s^{-1}) and (b) downward cloud mass flux (kg m^{-3} m s^{-1}) averaged over the horizontal domain. Vertical profiles of (c) total water flux (W m^{-2}), and (d) buoyancy flux (W m^{-2}) horizontally averaged over the cloud updraft region.

change is zero in the control/rad run. The maximum value of cloud liquid water has a net decrease from 1.8 to 1.3 g kg^{-1} in all the runs. The drizzle simulations also result in about 25% reduction in vertical velocity in the cloud updraft region (Fig. 7d) in addition to the height differences.

The reason that deeper clouds occur in the drizzle runs is likely due to small amounts of drizzle initially providing cooling just below cloud base and stabilization. This allows the buildup of convective available potential energy, which results in larger and stronger eddies. The results are consistent with the drizzling cumulus-under-stratus simulations of Stevens et al. (1998), though different in intensity.

The cloud mass flux (σw, where σ denotes the cloud fractional area) (Fig. 8a) shows a strong resemblance to the cloud cover (Fig. 7a) distribution, although the strongest w (Fig. 7d) is located near the inversion layer. The smallest amount of cloud layer mass flux is simulated in the drizzle/rad run, due to the reduced w compared to the control run. The significantly less mass flux is largely related to less cloud cover (Fig. 7a) in the drizzle/rad run. The maximum value of cloud mass flux in the downdraft region (Fig. 8b) is about 10% of that in the updraft region, and the strongest is obtained in the drizzle run. Both the total water flux (Fig. 8c) and the buoyancy flux (Fig. 8d) (actually flux of virtual potential temperature) in the updraft region show that there is a general reduction when the prescribed longwave radiative cooling is replaced by the two-stream radiation scheme, while drizzle results in further reduction in the fluxes as well.

The three-dimensional fields of cloud and rain water provide another perspective of the simulated clouds. Figure 9 shows the 0.001 g kg^{-1} surface of cloud water mixing ratio in both the control/rad and drizzle/rad runs in the cloud layer, along with the 0.01 g kg^{-1} surface of rain mixing ratio below cloud base in the drizzle/rad run, at 180 min from the beginning of the simulation. At this time, more clouds exist and cover a larger volume in the drizzle/rad run, with drizzle falling directly underneath the deepest clouds compared to the control/rad run. Several shallower cumuli exist as well in the drizzle/rad run.

The longwave radiative cooling produced by the radiative scheme shows similar features in both control/rad and drizzle/rad runs (Fig. 10), suggesting that the differences in the above simulations are due to the in-

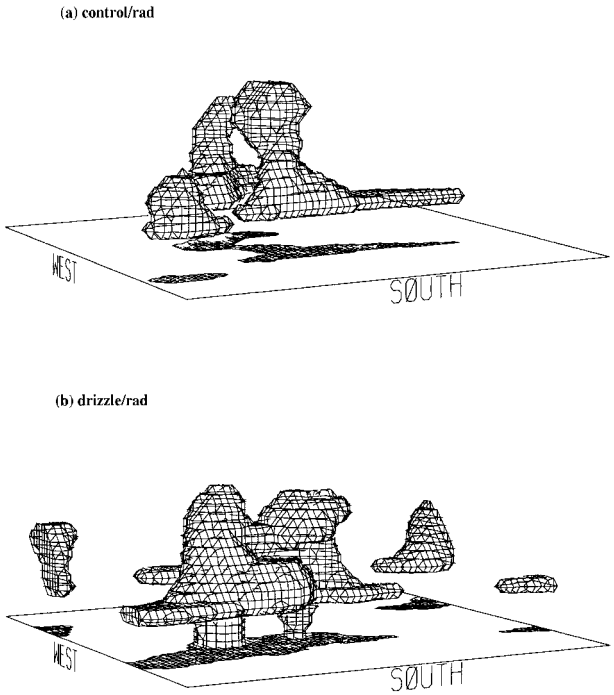

FIG. 9. The 0.001 g kg^{-1} cloud water surface at 180 min for (a) the control/rad run, and (b) the drizzle/rad run. View is from the southwest. Vertical projection of the cloud is shown at the surface. In (b) the 0.01 g kg^{-1} rainwater surface is also included below cloud base.

teraction between the microphysics and the radiation. Maximum cooling of approximately 3 K day^{-1} occurs between 600 and 700 m, the height corresponding to the top of the majority of shallow cumuli (e.g., see Fig. 7a). Approximately 2 K day^{-1} cooling is present through most of the cloud layer. The cooling starts decreasing from 2 K day^{-1} at 1500 m to 1 K day^{-1} at 2500 m. Note the prescribed cooling reduces to zero at 2500 m (Fig. 1b) in the control and drizzle runs.

5. Summary and discussion

In this paper, we have examined the role of precipitation in shallow marine cumulus convection in the trade wind region with a number of large eddy simulations in conjunction with the intercomparison project of the GCSS boundary layer working group. We have also examined in some detail the sensitivity of trade wind cumuli to radiative effects and the interaction between the radiation and precipitation.

The major results of the present study may be summarized as follows. The simulation results without parameterization for explicit microphysics and interactive radiation (control run) compare reasonably well with the intercomparison group when averaged over the last 3 h, although the RAMS simulation is the most active one in terms of turbulent fluxes [comparisons to others in the group are not shown but were reported in the boundary layer group workshop held in Seattle, Washington, in July 1997 and can be found online (www.knmi.nl/~siebesma/bomex.html)]. Similar features are produced when a bulk microphysics parameterization is included in the drizzle run.

Domain-averaged fields that are not directly related to, or being affected by, the liquid water field, such as x component of momentum fluxes and horizontal velocity variances, do not show significant differences between the control run and the drizzle run, owing to the fact that the drizzle mixing ratio only contributes about 2% to the total liquid water content. However, detailed analysis reveals that changes are prevalent during the last 3 h of simulation. A much larger buoyancy flux in the control run allows significant amounts of TKE to be transported to the inversion layer to do the work against buoyancy necessary for entrainment to proceed. Consequently, there is more entrainment in the control run than in the drizzle run. Heavy drizzle events are simulated in association with clouds that are deeper than 2 km, even though the majority of clouds are only a few hundred meters deep. The averaged surface precip-

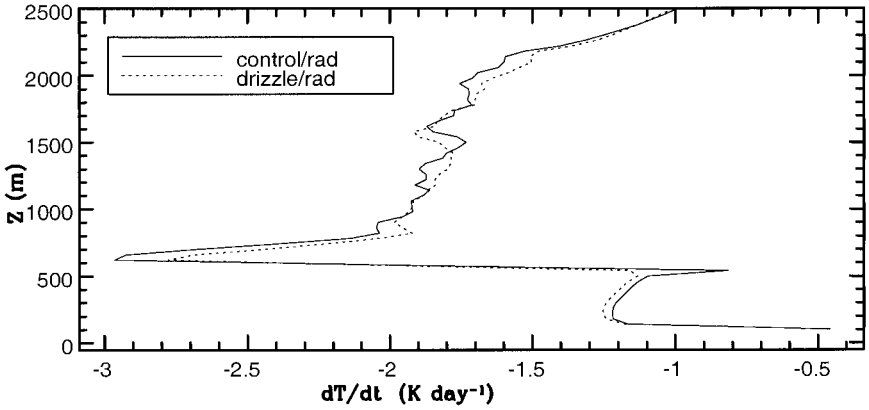

FIG. 10. Longwave radiative cooling averaged over the last 3 h of simulation for the control/rad run and drizzle/rad run.

itation rate in the drizzle run is in agreement with that observed. Albeit very slight, the presence of drizzle results in a reduction in $\langle w'w' \rangle$ as well as a weaker buoyancy production of TKE. This is consistent with the simulation of a drizzling marine stratocumulus boundary layer by Stevens (1996) and Stevens et al. (1998). They also found that drizzle reduced $\langle w'w' \rangle$ and buoyancy production of TKE, as well as the bulk entrainment rate in the boundary layer, although drizzle had a much stronger effect there.

For this GCSS study, it was assumed that cloud systems will reach a steady state, that is, time-independent profiles of the cloud fields after 2 h of simulation. Most of the results, however, exhibit considerable temporal fluctuations in the fluxes over the last 3 h, implying that the simulation domain is perhaps too small to average out the effects of the individual life cycle of clouds. Holland and Rasmusson (1973) pointed out that the atmospheric conditions cannot be characterized as steady as the intensity and height of the trade inversion varied considerably during BOMEX phase III, although they were described as undisturbed.

Overall, the impact of drizzle on shallow marine cumulus clouds in the trade wind region is small, as one would expect. Nevertheless, the results of this study can be useful for any future modeling studies, intercomparison projects, and the boundary layer community.

However, when the prescribed longwave radiative cooling is replaced with an interactive two-stream radiation parameterization, the boundary layer grows deeper and, as a result, a heavier drizzle event is simulated. The heavy drizzle reduces the liquid water content significantly. The evaporation of falling drizzle cools and moistens the lower levels of the cloud layer and the subcloud layer. A linear distribution of total water flux suggests that a relatively steady state has been reached in the drizzle/rad run.

The hydrometeor spectrum is broadened by including drizzle. For a given amount of condensate, absorption of IR radiation is greater in a drizzling cloud than in a nondrizzling cloud. Furthermore, the fact that only minor differences are obtained between the control run and the control/rad run suggests that drizzle leads to a change in cloud structure that has a strong effect on the amount of radiation absorbed and where that radiation is deposited in the cloud. Thus, the dynamics of the cloud and the boundary layer is altered.

Acknowledgments. Thanks are given to Ray McAnelly for his careful and constructive review of this manuscript as well as for his help to create the three-dimensional figure. B. Stevens is thanked for his help with initial model setup used for the intercomparison project. R. Walko is thanked for his help with every model-related question. The comments of S. Krueger and two anonymous reviewers greatly improved the clarity of this manuscript. This research is supported by the National Science Foundation through Grant ATM-9529321.

REFERENCES

Browning, K. A., Ed., 1994: *GEWEX Cloud System Study (GCSS) Science Plan.* IGPO Publication Series, Vol. 11, World Climate Research Programme International GEWEX Project Office, 84 pp.

Davidson, B., 1968: The Barbados Oceanographic and Meteorological Experiment. *Bull. Amer. Meteor. Soc.,* **49,** 928–934.

Dharssi, I., R. Kershaw, and W. K. Tao, 1997: Sensitivity of a simulated tropical squall line to long-wave radiation. *Quart. J. Roy. Meteor. Soc.,* **123,** 187–206.

Feingold, G., R. L. Walko, B. Stevens, and W. R. Cotton, 1998: Simulations of marine stratocumulus using a new microphysical parameterization scheme. *Atmos. Res.,* **47–48,** 505–528.

Harrington, J. Y., T. Reisin, W. R. Cotton, and S. M. Kreidenweis, 1999: Cloud resolving simulations of Arctic stratus. Part II: Transition-season clouds. *Atmos. Res.,* **51,** 45–75.

Holland, J. Z., and E. M. Rasmusson, 1973: Measurement of the atmospheric mass, energy, and momentum budgets over a 500-kilometer square of tropical ocean. *Mon. Wea. Rev.,* **101,** 44–55.

Mason, B. J., 1971: *The Physics of Clouds.* Oxford University Press, 671 pp.

Meyers, M. P., R. L. Walko, J. Y. Harrington, and W. R. Cotton, 1997: New RAMS cloud microphysics parameterization. Part II: The two-moment scheme. *Atmos. Res.,* **45,** 3–39.

Mitchell, D. L., A. Macke, and Y. Liu, 1996: Modeling cirrus clouds. Part II: Treatment of radiative properties. *J. Atmos. Sci.,* **53,** 2967–2988.

Moeng, C.-H., and Coauthors, 1996: Simulation of a stratocumulus-topped planetary boundary layer: Intercomparison among different numerical codes. *Bull. Amer. Meteor. Soc.,* **77,** 261–278.

Nicholls, S., and M. A. LeMone, 1980: The fair weather boundary layer in GATE: The relationship of subcloud fluxes and structure to the distribution and enhancement of cumulus clouds. *J. Atmos. Sci.,* **37,** 2051–2067.

——, and ——, 1982: The simulation of a fair weather marine boundary in GATE using a three-dimensional model. *Quart. J. Roy. Meteor. Soc.,* **108,** 167–190.

Nitta, T., and S. Esbensen, 1974: Heat and moisture budget analyses using BOMEX data. *Mon. Wea. Rev.,* **102,** 17–28.

Pennel, W. T., and M. A. LeMone, 1974: An experimental study of turbulent structure in the fair-weather trade wind boundary layer. *J. Atmos. Sci.,* **31,** 1308–1323.

Pielke, R. A., and Coauthors, 1992: A comprehensive meteorological modeling system—RAMS. *Meteor. Atmos. Phys.,* **49,** 69–91.

Ritter, B., and J. F. Geleyn, 1992: A comprehensive radiation scheme for numerical weather prediction models with potential application in climate simulations. *Mon. Wea. Rev.,* **120,** 303–325.

Siebesma, A. P., and J. W. M. Cuijpers, 1995: Evaluation of parametric assumptions for shallow cumulus convection. *J. Atmos. Sci.,* **52,** 650–666.

Slingo, A., and H. M. Schrecker, 1982: On the shortwave radiative properties of stratiform water clouds. *Quart. J. Roy. Meteor. Soc.,* **108,** 407–426.

Soong, S.-T., and Y. Ogura, 1980: Response of tradewind cumuli to large-scale processes. *J. Atmos. Sci.,* **37,** 2035–2050.

Stevens, B., 1996: On the dynamics of precipitating stratocumulus. Ph.D. dissertation, Colorado State University, 140 pp. [Available from Dept. of Atmospheric Sciences, Colorado State University, Fort Collins, CO 80523.]

——, W. R. Cotton, G. Feingold, and C.-H. Moeng, 1998: Large-eddy simulations of strongly precipitating, shallow, stratocu-

mulus-topped boundary layers. *J. Atmos. Sci.,* **55,** 3616–3638.
Stull, R. B., 1988: *An Introduction to Boundary Layer Meteorology*. Kluwer Academic, 666 pp.
Tao, W., J. Simpson, C. Sui, B. Ferrier, S. Land, J. Scala, M. Chou, and K. Pickering, 1993: Heating, moisture, and water budgets of tropical and midlatitude squall lines: Comparisons and sensitivity to longwave radiation. *J. Atmos. Sci.,* **50,** 673–890.
Tiedtke, M., 1989: A comprehensive mass flux scheme for cumulus parameterization in large-scale models. *Mon. Wea. Rev.,* **117,** 1779–1800.
Tripoli, G. J., and W. R. Cotton, 1981: The use of ice-liquid water potential temperature as a thermodynamic variable in deep atmospheric models. *Mon. Wea. Rev.,* **109,** 1094–1102.
Walko, R. L., W. R. Cotton, M. P. Meyers, and J. Y. Harrington, 1995: New RAMS cloud microphysics parameterization. Part I: The single-moment scheme. *Atmos. Res.,* **38,** 29–62.